Chemical Engineering Journal 101 (2004) 303–314

Chemical Engineering Journal

www.elsevier.com/locate/cej

Modeling of electric-field driven transport processes in microdevices for immunoassay

Michal Přibyl*, Dalimil Šnita, Pavel Hasal, Miloš Marek

Department of Chemical Engineering, Center for Nonlinear Dynamics of Chemical and Biological systems, Institute of Chemical Technology, Prague, Czech Republic

Received 25 July 2003; accepted 28 October 2003

Abstract

This work is focused on mathematical modeling of reaction-transport processes in a microdevice for immunoassay. A mathematical model of a four-layer microdevice for a multiple enzyme-linked immunosorbent assay (ELISA) analysis in a serial configuration is proposed. Effects of electrokinetic transport and some significant parameters (e.g. antibody effective diffusivity/mobility, convective velocity, fixed charge in a porous membrane) on the immunoassay procedure are studied. The mathematical model includes component balances and Poisson equation of electrostatics. Steady-state analysis shows qualitative effects of the model parameters on the concentration of antibody in the reaction area. Dynamical analysis quantitatively reveals effects of crucial parameters on the time needed for the immunoassay procedure. It was observed that this time can be reduced to several minutes by a proper choice of control parameters. One complete step of ELISA application in the series arrangement of probes is analyzed in detail.

Keywords: Immunoassay; ELISA; Microchip; Electrophoresis; Electroosmosis; Modeling

1. Introduction

Immunoanalytical methods are widely used in disease diagnostics (e.g. viral or bacterial infections, cancer, thrombosis), screening of environmental pollution, detection of weapons of mass destruction (chemical and biological weapons), etc. [1]. Immunoassays are based on a complementary non-covalent reaction between an antigen and a corresponding antibody. A frequently used immunoanalytical method is enzyme-linked immunosorbent assay (ELISA). Either an antigen or an antibody is immobilized on a sorbing matrix. The complementary compound in a sample, usually tagged by a detectable molecule, binds firmly to the molecules in the matrix. After elution of excess complementary molecules, an antigen–antibody complex in the matrix can be detected by a standard bioanalytical method. Commercially successful are sandwich ELISA methods. For example, an immobilized antigen binds a primary human antibody from a sample. After the first elution, a secondary antibody, for example a tagged rabbit antibody against the human antibodies, is introduced to the primary antibody–antigen complex. The secondary antibody forms a secondary antibody—primary antibody—antigen complex. After the second elution, this complex can be detected by any suitable method.

Recent expansion in the use of DNA chips [2] and capillary electrophoresis [3,4] motivates efforts to further develop immunoassay chips. Microchips open new possibilities in immunoanalysis applications. Most steps of the immunoassay procedure can be integrated within a simple chip [5]. Other benefits of bio-microdevices are ease of massive paralelization, low consumption of expensive chemicals, and better reproducibility.

Many experimental microchips for immunoassay (especially for ELISA) were recently described [5–14]. Dodge et al. [5] constructed an experimental ELISA microchip with a high degree of integration. This microdevice is able to detect the rabbit immunoglobulin G (antibody) by means of the protein A (antigen) immobilized in the reaction part of the microchip. The following steps of immunoassay procedure are done electrokinetically: sample dosage, washing and elution of the antibody. The device integrates sample dosage, incubation, washing, detection, and elution. The time of the incubation phase is less than 5 min. The described device can be used several times and its parallelization is probably possible.

* Corresponding author. Tel.: +420-2-2435-3168; fax: +420-2-3333-7335.
E-mail address: michal.pribyl@vscht.cz (M. Přibyl).

1385-8947/$ – see front matter © 2004 Elsevier B.V. All rights reserved.
doi:10.1016/j.cej.2003.10.013

The sample dosage and flow inside the microdevice can be effectively controlled by electrokinetic phenomena: electrophoresis and electroosmosis [5,11,12]. If an external electric field is imposed on a microchannel structure, the electroosmotic flow of the solution occurs in the microchip structure because of charge bound to microchannel walls and/or in a porous matrix. Electrokinetic transport can be dominant within microchannels. This possibility is given by a high intensity of transport of the Joule heat out of the device when a high voltage is applied [2]. A suitable intensity of the electric field and its spatial orientation can result in a local increase of antibody (antigen) concentration in the matrix with the immobilized complementary compound, hence the time needed for the immunoassay decreases.

Most of the publications describe experiments on microchips for immunoanalytical applications. Construction of such a microdevice often involves a lot of trial and error. Thus mathematical modeling of processes inside the microdevices can become a useful tool for acceleration of the development of bio-microapplications. However, mathematical description of such microsystems is not an easy task. It usually means to solve appropriate mass balances of components and equations for distribution of electrostatic potential, velocity, and pressure in the microsystem. It is still a non-trivial problem, especially if 2D or 3D spatiotemporal patterns are to be computed.

Ermakov et al. [15,16] numerically studied the electrokinetic transport mechanisms in microvalves (two microchannels in the cross arrangement). These microvalves can be used for sample injection in a microchip. The authors determined a voltage for maximal concentration of a compound in a sample. Li [17] focused on a detailed mathematical description of the electrokinetic phenomena in microchannels and their impacts on the behavior of the microsystem. The author deals with the properties of an electrical double layer. Electroviscous effects and impacts of the electrokinetic transport on velocity distribution inside the channel are also described. Lindner et al. [18] studied distributions of component concentrations and electrostatic potential in a simple system with a narrow acid–base boundary. The authors found that such a system can exhibit diode-like behavior. Similar phenomena are usually observed, under certain conditions, near a liquid–solid phase interface (i.e., in every ELISA system). Khandurina et al. [19] demonstrate the use of semipermeable membranes to concentrate a macromolecular analyte. We speculate that an ELISA system can contain a semipermeable membrane directly at the reaction compartment to accelerate the entire immunoassay procedure.

In the first part of the paper, we propose a general system for the ELISA application with a corresponding simplified mathematical description. Our analysis is focused on both the steady-state and dynamical analysis of the system. In the final part, we provide and discuss result of simulation for one complete immunoassay cycle.

2. Mathematical model

Our mathematical model is derived for the microdevice shown in Fig. 1. The proposed biochip integrates all steps usually contained in the immunoassay. Let us assume that the sandwich ELISA procedure can be realized in series in a single channel with connected detection probes. The order of particular steps during the immunoassay is shown in Fig. 1A. A sample with a primary antibody or a tagged secondary antibody is introduced into the central microchannel of the system. The sample is then directly addressed into a chosen probe. Each probe contains two porous compartments. The reaction and detection environments form the first one. An antigen is immobilized within a thin gel layer. After some time, the antibody from the sample and the immobilized antigen form an antigen–antibody complex. The other porous compartment is a semipermeable membrane. This compartment is located immediately behind the reaction environment. The semipermeable membrane has two important functions. The membrane is completely impermeable for large molecules such as antibodies and thus helps to concentrate the antibody in the reaction compartment. The polymer matrix of the semipermeable membrane can contain a large amount of fixed electrostatic charge. This property is necessary to induce electroosmotic convection in the system

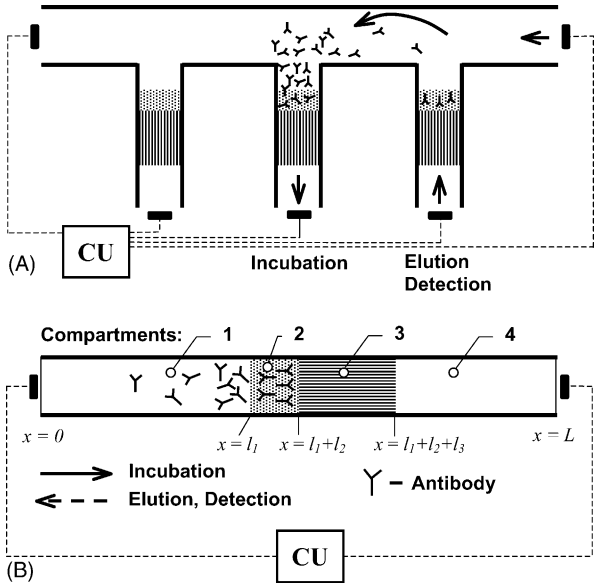

Fig. 1. (A) Microdevice for an immunoassay with probes in series. Spatially 2D system with three immunoanalytical probes. The control unit (CU) controls the electroosmotic convection and the electromigration transport in the system by means of voltage control in the entire system. The sample is released from the right probe where the antibody detection can start. At the same time, the antigen–antibody incubation reaction occurs in the middle probe. The left probe is ready for analysis. (B) The scheme of a single probe. The probe consists of four compartments. Numbers 1, 2, 3, and 4 denote the input compartment, the reaction compartment, the semipermeable compartment, and the output compartment, respectively. The arrows show directions of the antibody total flux that are necessary for the incubation and elution phases of an ELISA application.

if an external electric field is applied. After the incubation reaction in the first probe, the sample with the antibody can be re-addressed to the next probe. At the same time, excess antibody from the first probe is released and the detection of the antigen–antibody complex can start. This procedure can be repeated for all chosen probes in the microchannel. The addressing occurs via electrokinetic effects (electroosmosis and/or electrophoresis) and/or by a pressure gradient. The electroosmotic transport of the carrying solution can be the dominant transport phenomenon in the system when a microporous semipermeable membrane with fixed electrostatic charge is used. Then, a unit for voltage control (CU) can serve as an efficient tool for antibody addressing.

We first focus on a steady-state and dynamical analysis of a single probe (see Fig. 1B). This probe consists of four layers. A solution with a sample is introduced through the input compartment. The second and the third layers are the reaction compartment and semipermeable membrane, respectively. The last compartment contains an output solution free of antibody. The required direction of the antibody transport is from the input compartment to the reaction compartment during the incubation phase. The opposite direction of transport is necessary for elution of the excess antibody. Our task is to find a proper set of parameters to attain an efficient transport of the antibody during both the incubation and the elution phases, because high concentration of the antibody in the reaction compartment is the key for the decrease of the operation time of the immunoassay.

We consider the following components in the ELISA system: antibody ($Ab^{z_{Ab}}$), antibody–antigen complex ($C^{z_{Ab}}$), the buffer in both the electroneutral (B) and the electrically charged (protonized) forms (Bp^+), the chloride counterion (Cl^-) of the protonized form of buffer, hydroxyl ions (OH^-) and protons (H^+). The total concentration of the antigen (Ag) in the reaction environment is the sum of the concentration of the free antigen and the concentration of the antigen–antibody complex, and this sum is constant in time and space. The Tris buffer, which is typically used in the ELISA applications, was chosen as a model buffer. The superscripts denote the charge numbers of a particular compound. The antibody molecules can posses varying charge number z_{Ab}. In our study, we have considered z_{Ab} as a model parameter. It is assumed that the charge number of the antibody is equal to the charge number of the antigen–antibody complex because the antigen is considered to be electroneutral. For simplicity, the charge numbers are omitted from the subscripts in equations and tables.

There are three chemical/biochemical interactions in the proposed system:

$$H_2O \overset{K_w}{\rightleftarrows} H^+ + OH^-, \quad Bp^+ \overset{K_b}{\rightleftarrows} H^+ + B, \quad C^{z_{Ab}} \overset{K_c}{\rightleftarrows} Ab^{z_{Ab}} + Ag,$$

the recombination reaction of water, buffer dissociation/association reaction and the antigen–antibody formation/dissociation reaction, respectively. The first two interactions occur in the entire system, the antigen–antibody interaction is limited only to the reaction domain with immobilized antigen.

Each probe of the ELISA system is generally 3D in space. However, the transport in the directions perpendicular to the longitudinal axis (see Fig. 1B) can be considered as fast in most cases because of a low ratio of the lateral to longitudinal dimension of the system (the ratio is expected to be of the order of 1/50). Hence, we use spatially 1D description of the proposed system.

The non-stationary molar balance can be written in the standard form,

$$\frac{\partial c_i}{\partial t} = -\frac{\partial J_i}{\partial x} + \sum_j \upsilon_{ij} r_j, \quad i = H^+, OH^-, Cl^-, B, Bp^+, C^{z_{Ab}}, Ab^{z_{Ab}}. \tag{1}$$

From the left, there are three terms in the balance: the accumulation term, the term describing divergence of total flux J_i, and the sum of all reaction sources for the compound i. Eq. (1) is used in the whole system for most of the components. There are two exceptions: (1) The antibody molecules are limited to the input and the reaction compartments because of the presence of the semipermeable membrane. (2) The molecules of the antigen–antibody complex are strictly located in the reaction compartment.

The total flux of the component i is given by the sum of convection, diffusion, and electromigration fluxes

$$J_i = J_i^C + J_i^D + J_i^E = v_x c_i - D_i \frac{\partial c_i}{\partial x} - \frac{z_i D_i F}{RT} c_i \frac{\partial \Phi}{\partial x}, \quad i = H^+, OH^-, Cl^-, B, Bp^+, Ab^{z_{Ab}}. \tag{2}$$

The velocity of the liquid flow v_x is constant in this 1D incompressible system so that the continuity equation is satisfied. This fact significantly reduces the complexity of description since Navier–Stokes equations are eliminated and the convection velocity becomes only a fixed parameter of the model. In this case, the resulting velocity of liquid flow can be considered as a sum of the velocity of electroosmotic flux and the velocity given by an external pressure gradient.

The Nernst–Planck equation is used for the description of the diffusion and the electromigration fluxes in Eq. (2). Let us note that the description of electromigration of macroobjects such as antibodies by means of the Nernst–Planck equation is only approximate. The electrophoretic motion of a charged particle moving in a fluid under the action of an applied electric field can be described by the Helmholtz–Smoluchowski equation [20]

$$v_{xe} = -\frac{\varepsilon \zeta_E}{\mu} \frac{\partial \Phi}{\partial x}, \tag{3}$$

where the v_{xe} is the electrophoretic velocity, ε the permittivity of the environment, μ the viscosity of the electrolyte and ζ_E the electrophoretic zeta potential. The value of the zeta potential is a property of the macromolecule (antibody) and depends also on the composition of the surrounding

electrolyte. Determination of the zeta potential is generally difficult and is usually based on carefully evaluated experiments. If we look at the electrophoretic velocity used in the Nernst–Planck expression

$$v_{xe} = -\frac{z_{Ab} D_{Ab} F}{RT} \frac{\partial \Phi}{\partial x}, \tag{4}$$

we can accept a formal simplification that the product $z_{Ab}D_{Ab}$ in Eq. (4) is proportional to the zeta potential and to material properties (such as viscosity and permittivity) in Eq. (3). Then we can assume that z_{Ab} is an effective charge number that can be generally non-integer. Similarly, the diffusion coefficient D_{Ab} in Eq. (4) is an effective diffusion coefficient D_{Ab}^{ef} that generally does not correspond to the diffusion coefficient D_{Ab} in the Fick's law of diffusion. In our numerical simulations, we have set $D_{Ab}^{ef} \approx D_{Ab}$. The description of electromigration by means of Eq. (4) is thus formally equivalent to the description by Eq. (3).

All parameter values of this model are summarized in Table 1 and in the figure captions. Because the diffusivities of larger molecules differ in a free solution of electrolyte and in a porous medium, we have used lower (effective) values of diffusion coefficients in both the reaction and the semipermeable compartment than in the input/output solutions. These diffusion coefficients are marked by the superscript 'p'.

The expressions for reaction rates of the chemical/biochemical reactions mentioned above are written as

$$r_w = k_w(K_w - c_H c_{OH}), \qquad r_b = k_b(K_b c_{Bp} - c_H c_B),$$
$$r_c = k_c(K_c c_C - c_{Ab}(c_{Ag,tot} - c_C)), \tag{5}$$

where r_w is the reaction rate of the recombination reaction of water, r_b the reaction rate of buffer dissociation/association reaction and r_c the reaction rate of the antigen–antibody formation/dissociation reaction (see Table 1 for values of kinetic and equilibrium constants). The assumption of an instantaneous equilibrium of the water and buffer reactions is not used. We consider finite rates of these interactions.

The electromigration of charged components (Cl^-, Bp^+, OH^-, H^+, $Ab^{z_{Ab}}$) depends on the distribution of electrostatic potential Φ in the system. This distribution can be

Table 1
Model parameters

Parameter	Description	Value	Units
$c_H\|_{x=0,L}$	Boundary concentrations of protons	1×10^{-5}	mol m^{-3}
$c_{OH}\|_{x=0,L}$	Boundary concentrations of hydroxyl ions	1×10^{-3}	mol m^{-3}
$c_{Cl}\|_{x=0,L}$	Boundary concentrations of chloride ions	3.331×10^{1}	mol m^{-3}
$c_B\|_{x=0,L}$	Boundary concentrations of buffer	1.669×10^{1}	mol m^{-3}
$c_{Bp}\|_{x=0,L}$	Boundary concentrations of protonized buffer	3.331×10^{1}	mol m^{-3}
$c_{Ag,tot}$	Total concentration of the immobilized antigen	1×10^{-3}	mol m^{-3}
$\Phi\|_{x=L}$	Electrostatic potential on the boundary	0	V
D_H, D_H^p	Diffusion coefficient of protons	9.31×10^{-9}	m^2 s^{-1}
D_{OH}, D_{OH}^p	Diffusion coefficient of hydroxyl ions	5.28×10^{-9}	m^2 s^{-1}
D_{Cl}	Diffusion coefficient of chloride ions in a free solution	2.04×10^{-9}	m^2 s^{-1}
D_B, D_{Bp}	Diffusion coefficient of buffer in a free solution	3.734×10^{-10}	m^2 s^{-1}
D_{Cl}^p	Diffusion coefficient of chloride ions in a porous medium	1.02×10^{-9}	m^2 s^{-1}
D_B^p, D_{Bp}^p	Diffusion coefficient of buffer in a porous medium	1.867×10^{-10}	m^2 s^{-1}
l_1	Length of the input compartment	2×10^{-4}	m
l_2	Length of the reaction compartment	1×10^{-5}	m
l_3	Length of the semipermeable compartment	1×10^{-4}	m
l_4	Length of the output compartment	2×10^{-4}	m
$L = \sum_{i=1}^{4} l_i$	Dimension of the system	5.1×10^{-4}	m
z_H	Charge number of protons	1	1
z_{OH}	Charge number of hydroxyl ions	−1	1
z_{Cl}	Charge number of chloride ions	−1	1
z_B	Charge number of buffer	0	1
z_{Bp}	Charge number of protonized buffer	1	1
z_{Ag}	Charge number of the immobilized antigen	0	1
F	Faraday's constant	9.6487×10^{4}	C mol^{-1}
R	Molar gas constant	8.314	J mol^{-1} K^{-1}
T	Temperature	310	K
k_w	Kinetic constant of water recombination	1.3×10^{8}	m^3 mol^{-1} s^{-1}
K_w	Ionic product of water	1×10^{-8}	mol^2 m^{-6}
k_b	Kinetic constant of buffer protonization	1.3×10^{7}	m^3 mol^{-1} s^{-1}
K_b	Equilibrium constant of buffer dissociation	5.012×10^{-6}	mol m^{-3}
k_c	Kinetic constant of antigen–antibody complex formation	1×10^{5}	m^3 mol^{-1} s^{-1}
K_c	Equilibrium constant of antigen–antibody complex formation	1×10^{-7}	mol m^{-3}
ε_0	Vacuum permittivity	8.8542×10^{-12}	F m^{-1}
ε_r	Relative permittivity of water	8.139×10^{1}	l

computed from the Poisson equation,

$$\varepsilon_r\varepsilon_0\frac{\partial^2\Phi}{\partial x^2} = -q_{mob} - q_{fix}, \tag{6}$$

where $\varepsilon_r\varepsilon_0$ denotes the permittivity that generally depends on the composition of the environment. Here we consider a constant permittivity in the entire system and in numerical simulations set it at water permittivity. The local charge in the Poisson equation consists of mobile charge carried by ions in the solution q_{mob} and volume charge bound in the porous/semipermeable matrix q_{fix}. The mobile charge is given by the local composition of the electrolyte according to Eq. (7)

$$q_{mob} = F\sum_i z_i c_i, \quad i = H^+, OH^-, Cl^-, Bp^+, C^{z_{Ab}}, Ab^{z_{Ab}}, \tag{7}$$

and the fixed charge is a property of the porous medium (generally depending on the composition of the mobile phase). In our computations, we consider a constant nonzero value of q_{fix} in the reaction and the semipermeable compartments.

We have chosen the following boundary conditions:

$$\begin{aligned}
&c_i|_{x=0} = c_{x0i}, \quad i = H^+, OH^-, Cl^-, B, Bp^+, Ab^{z_{Ab}},\\
&c_i|_{x=L} = c_{xLi}, \quad i = H^+, OH^-, Cl^-, B, Bp^+,\\
&J_{Ab}|_{x=l_1+l_2} = 0,\\
&c_i|_{x\to l_1-} = c_i|_{x\to l_1+}, \qquad J_i|_{x\to l_1-} = J_i|_{x\to l_1+},\\
&i = H^+, OH^-, Cl^-, B, Bp^+, Ab^{z_{Ab}},\\
&c_i|_{x\to (l_1+l_2)-} = c_i|_{x\to (l_1+l_2)+},\\
&J_i|_{x\to (l_1+l_2)-} = J_i|_{x\to (l_1+l_2)+},\\
&i = H^+, OH^-, Cl^-, B, Bp^+,
\end{aligned} \tag{8}$$

$$\begin{aligned}
&c_i|_{x\to (l_1+l_2+l_3)-} = c_i|_{x\to (l_1+l_2+l_3)+},\\
&J_i|_{x\to (l_1+l_2+l_3)-} = J_i|_{x\to (l_1+l_2+l_3)+},\\
&i = H^+, OH^-, Cl^-, B, Bp^+,\\
&\Phi|_{x=0} = \Phi_{x0}, \qquad \Phi|_{x=L} = \Phi_{xL},\\
&\Phi|_{x\to l_1-} = \Phi|_{x\to l_1+}, \qquad \Phi|_{x\to (l_1+l_2)-} = \Phi|_{x\to (l_1+l_2)+},
\end{aligned}$$

$$\begin{aligned}
&\Phi|_{x\to (l_1+l_2+l_3)-} = \Phi|_{x\to (l_1+l_2+l_3)+},\\
&\left.\frac{\partial\Phi}{\partial x}\right|_{x\to l_1-} = \left.\frac{\partial\Phi}{\partial x}\right|_{x\to l_1+},\\
&\left.\frac{\partial\Phi}{\partial x}\right|_{x\to (l_1+l_2)-} = \left.\frac{\partial\Phi}{\partial x}\right|_{x\to (l_1+l_2)+},\\
&\left.\frac{\partial\Phi}{\partial x}\right|_{x\to (l_1+l_2+l_3)-} = \left.\frac{\partial\Phi}{\partial x}\right|_{x\to (l_1+l_2+l_3)+}.
\end{aligned}$$

The Dirichlet boundary conditions are specified for electrostatic potential and all mobile components (except the antibody) on both external boundaries of the system (i.e., $x = 0$ and $x = L$). The antibody concentration is considered to be constant only on the input external boundary ($x = 0$). The condition of zero flux for the antibody is used on the interface between the reaction and the semipermeable compartments ($x = l_1 + l_2$). The other boundary conditions on all internal interfaces of the system ($x = l_1, x = l_1 + l_2, x = l_1 + l_2 + l_3$) follow existence of continuity in distributions of concentrations, total fluxes, electric potential, and electric field strength.

Eqs. (1), (6) and (8) form the system of model equations. These equations were transformed into dimensionless form that is more convenient for numerical analysis. The dimensionless form of model equations is given in Appendix A (see Table 2 for definition of dimensionless variables, dimensionless groups and scaling factors). Asterisks in superscripts of variables denote a dimensionless variable.

Table 2
Dimensionless variables and parameters, scaling factors

Dimensionless variables	
$x^* \equiv \frac{x}{x_0}$	Length
$v^* \equiv \frac{v_x}{v_0}$	Convection velocity
$c^*_{Ab} \equiv \frac{c_{Ab}}{c_{Ab}\|_{x=0}}$	Concentration of antibody
$c^*_i \equiv \frac{c_i}{\sqrt{K_w}}, i = H^+, OH^-$	Concentration of protons, and hydroxyl ions
$t^* \equiv \frac{t}{t_0}$	Time
$\Phi^* \equiv \frac{\Phi}{\Phi_0}$	Electrostatic potential
$c^*_C \equiv \frac{c_C}{c_{Ag,tot}}$	Concentration of complex
$c^*_i \equiv \left.\frac{c_i}{c_B}\right\|_{x=0}, i = Cl^-, B, Bp^+$	Concentration of chloride ions, buffer, and protonized buffer
Dimensionless parameters	
$Da_H = \frac{\sqrt{K_w}k_w l_2^2}{D_{Ab}}$	Damköhler number—water recombination
$Da_B = \frac{c_B\|_{x=0}k_b l_2^2}{D_{Ab}}$	Damköhler number—buffer dissociation
$Da_C = \frac{c_{Ag,tot}k_c l_2^2}{D_{Ab}}$	Damköhler number—complex formation
$D_i \equiv \frac{D_i}{D_{Ab}}$	Ratio of diffusion coefficients
$Q \equiv \frac{q_{fix}}{Fc_B\|_{x=0}}$	Ratio of the fixed charge and charge in the free electrolyte
$G \equiv \frac{c_B\|_{x=0}l_2^2F^2}{RT\varepsilon}$	Ratio of squares of the geometrical length and the Debye length
Scaling factors	
$x_0 = l_2$	
$t_0 = \frac{l_2^2}{D_{Ab}}$	
$v_0 = \frac{x_0}{t_0} = \frac{D_{Ab}}{l_2}$	
$\Phi_0 = \frac{RT}{F}$	

Let us note that we have neglected all temperature changes in our microdevice considering a high ratio of heat-exchange surface to internal volume.

3. Numerical analysis

Dimensionless model equations (see Appendix A) and their boundary conditions were analyzed by the method of finite elements. The FEMLAB2.3® package was employed in this study. A non-equidistant net of grid points was used in order to eliminate errors and computational problems near phase interfaces where sharp concentration and potential changes were observed. The ratio of lengths of the net elements in a flat region (e.g. the center of the input compartment) and at a phase interface (e.g. between the input and the reaction compartments) was 10^4. An implicit FEMLAB solver fldaspk (based on backward differentiation formulae) was used for dynamic analysis of the problem.

4. Results and discussion

4.1. Steady-state analysis

Effects of important model parameters on steady states of the proposed ELISA system were analyzed in the first step. Fig. 2 shows steady-state profiles of the dimensionless antibody concentration in the input compartment (i.e. $x^* \in (0; 20)$, see Appendix A) and the reaction compartment (i.e. $x^* \in (20; 21)$). Point $x^* = 20$ corresponds to the internal interface where the inlet compartment touches the reaction compartment and the boundary conditions (Eq. (8)) have to be satisfied. The effects of convective velocity, the effective charge number of the antibody and the imposed electrostatic potential are depicted. An antibody molecule is a typical ampholyte. Hence the effective charge number of the antibody can substantially affect the electrophoretic flux of biomacromolecules in the system.

When $z_{Ab} = 0$, we can observe the effect of convective velocity (Fig. 2A). In this arrangement with a fixed negative charge in the porous compartments and a positive electrostatic potential at the input boundary, the direction of the electroosmotic convection is oriented from the input to the output compartment. It means that v_x is positive. The electroosmotic flow of relatively low intensity ($v_x = 1\,\mu m\,s^{-1}$) can result in large increase of the antibody concentration in the reaction compartment (up to two orders of magnitude). This effect is amplified when the antibody carries a positive charge (see Fig. 2B). In this case, the effects of electroosmotic convection and electrophoretic migration are summed up. The resulting concentration of the antibody is then by six orders of magnitude higher than the inlet antibody concentration. It substantially increases reaction rate of the antigen–antibody complex formation. Let us note that the dimensionless antibody concentration $c^*_{Ab} \approx 1 \times 10^6$ corresponds to the antibody mass concentration of hundreds kilograms per cubic meter, which is the physical limit because of the possible formation of gel-like structures from the antibody molecules. On the other hand, such a large concentration of the antibody is attained only after very long time period. If we neglect both the diffusion transport and the antigen–antibody interactions and assume linear profile of potential through the system, $\partial\Phi/\partial x \approx (\Phi|_{x=L} - \Phi|_{x=0})/L$

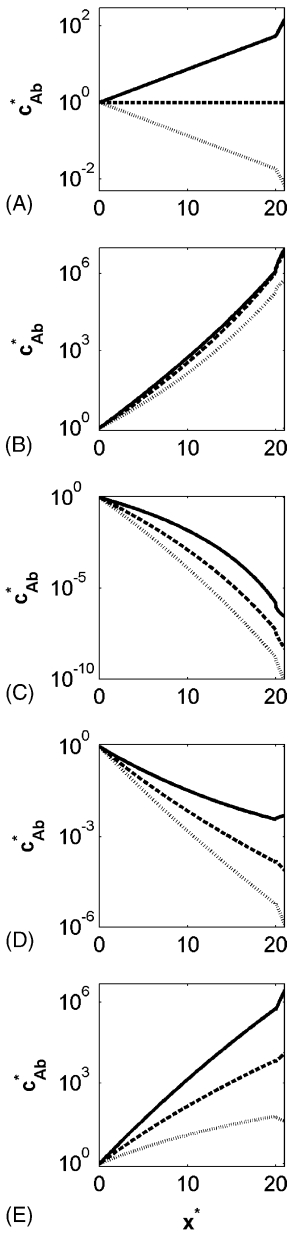

Fig. 2. Steady-state profiles of the dimensionless antibody concentration. Effects of antibody charge number, imposed potential, and convection velocity. (A) $\Phi|_{x=0} = 1\,V$, $z_{Ab} = 0$, (B) $\Phi|_{x=0} = 1\,V$, $z_{Ab} = 1$, (C) $\Phi|_{x=0} = 1\,V$, $z_{Ab} = -1$, (D) $\Phi|_{x=0} = -1\,V$, $z_{Ab} = 1$, (E) $\Phi|_{x=0} = -1\,V$, $z_{Ab} = -1$. $v_x = 1\,\mu m\,s^{-1}$ (solid line), $v_x = 0\,\mu m\,s^{-1}$ (dashed line), $v_x = -1\,\mu m\,s^{-1}$ (dotted line). The other model parameters are as in Table 1 and $c_{Ab}|_{x=0} = 4 \times 10^{-6}\,mol\,m^{-3}$, $q_{fix} = -1 \times 10^6\,C\,m^{-3}$, $D_{Ab} = 5 \times 10^{-11}\,m^2\,s^{-1}$, $D^p_{Ab} = D_{Ab}/5$.

we can compute time necessary to reach this concentration in the reaction environment. After reaching it, the total flux of the antibody in the input compartment is approximately equal to the accumulation of antibody in the reaction compartment,

$$t = \frac{n_{\mathrm{Ab}}|_{\mathrm{reaction\_comp}}}{A(J^{\mathrm{C}}_{\mathrm{Ab}} + J^{\mathrm{E}}_{\mathrm{Ab}})|_{x=0}} = \frac{c_{\mathrm{Ab}}(t)|_{\mathrm{reaction\_comp}} l_2}{(v_x c_{\mathrm{Ab}} - (z_{\mathrm{Ab}} D_{\mathrm{Ab}} F/RT)(\partial\Phi/\partial x) c_{\mathrm{Ab}})|_{x=0}}. \quad (9)$$

In Eq. (9), $n_{\mathrm{Ab}}|_{\mathrm{reaction\_comp}}$ is the total molar amount of the antibody accumulated in the reaction compartment, A the surface of the probe cross-section. For our set of parameters, the required time is about 24 days, which fully corresponds with the results of dynamical simulations. Hence, the computations of steady states can be used only as a tool for qualitative predictions of the effects of various model parameters on global behavior of the system.

Results for other combination of the imposed electrostatic potential and charge number are shown in Fig. 2C–E. Generally, if the direction of electrophoretic migration (depends on the antibody charge number and the electric field orientation) is from the input compartment to the reaction compartment, a substantial increase of the antibody concentration in the reaction compartment is observed (Fig. 2B and E). This regime is required for the incubation phase of the ELISA procedure. A decrease of the antibody concentration in the reaction compartment occurs if the opposite orientation of electrophoretic migration of the antibody is considered (Fig. 2C and D). Such a regime prevails during the elution/detection phase of the ELISA application. Electroosmotic convection or convection induced by an external pressure gradient may strongly affect the resulting antibody concentration. But the velocity of the convection flow of the order of $1\,\mu\mathrm{m\,s^{-1}}$ is relatively small. For higher values of the convective velocity, other phenomena can be observed. For example, a full suppression of electrophoretic migration of the antibody by electroosmotic convection, etc.

The solid line in Fig. 3A shows the steady-state distribution of the electrostatic potential in the entire probe when no electrostatic charge is fixed in the reaction and the semipermeable compartments $x^* \in (20; 31)$. We can see that this profile is piece-wise linear. The slope of the decrease of the potential is higher in the porous compartments because of lower diffusivities of the key ions (the chloride anions and the protonized form of the buffer). For example, the chloride anions are not consumed in any chemical transformation and thus their total flux has to be constant in the whole system. It implies that a lower diffusivity of the chloride anions is compensated by a higher value of the electric field intensity $E \equiv -\partial\Phi/\partial x$ in the central region of the ELISA probe. The corresponding profiles of the electric field intensity and the dimensionless antibody concentration are shown in Fig. 3B and C. For clarity, the Fig. 3B is focused only on the interface between the input and the reaction compartment.

Local phenomena at the phase interface (input solution/reaction environment) caused by the presence of the fixed charge in the porous compartments also affect the antibody concentration in the reaction compartment. For that reason, behavior of the proposed ELISA system is asymmetric (see differences between Fig. 2B and E and between Fig. 2C and D). The effects of the fixed charge become important when the amount of the fixed charge is comparable with the amount of electrostatic charge carried by the components of the electrolyte,

$$cF \approx |q_{\mathrm{fix}}|, \quad (10)$$

where c is a characteristic chemical concentration of ions in the electrolyte. When $q_{\mathrm{fix}} = -1 \times 10^5\,\mathrm{C\,m^{-3}}$, effects of the fixed charge on behavior of the system are negligible. However, when the values of the fixed negative charge are higher by one order of magnitude, much faster decrease of the electrostatic potential near the interface of the input and the reaction compartments can be observed. Electric field intensities higher than $1\,\mathrm{MV\,m^{-1}}$ are observed near the interface (see Fig. 3B).

This phenomenon can be explained as follows. The protonized form of the buffer (the dominant cation) is strongly attracted to the interface in the region with the fixed negative charge. For a given orientation of the electric field, the resulting direction of total flux of the protonized buffer is from the input compartment to the output compartment. This flux has to be approximately constant in the whole system (there

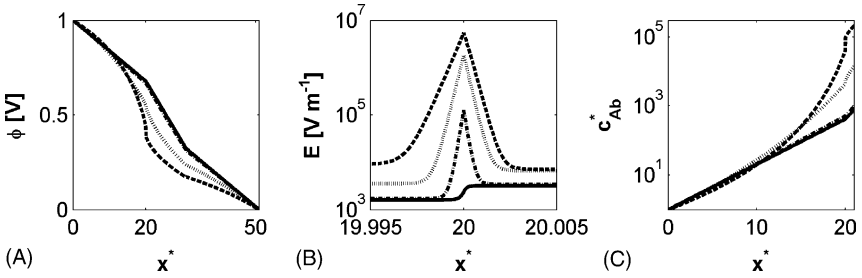

Fig. 3. Steady-state distribution of electrostatic potential in the whole system (A), the local steady-state profile of the electric field intensity $E \equiv -\partial\Phi/\partial x$ (B), and steady-state profiles of dimensionless antibody concentration in the input and the reaction compartments (C). Effects of the fixed charge: $q_{\mathrm{fix}} = 0\,\mathrm{C\,m^{-3}}$ (solid line), $q_{\mathrm{fix}} = -1 \times 10^5\,\mathrm{C\,m^{-3}}$ (dash-dotted line), $q_{\mathrm{fix}} = -1 \times 10^6\,\mathrm{C\,m^{-3}}$ (dotted line), $q_{\mathrm{fix}} = -2 \times 10^6\,\mathrm{C\,m^{-3}}$ (dashed line). The other model parameters are $v_x = 0\,\mu\mathrm{m\,s^{-1}}$, $z_{\mathrm{Ab}} = 0.5$, $\Phi|_{x=0} = 1\,\mathrm{V}$, $c_{\mathrm{Ab}}|_{x=0} = 4 \times 10^{-6}\,\mathrm{mol\,m^{-3}}$, $D_{\mathrm{Ab}} = 5 \times 10^{-11}\,\mathrm{m^2\,s^{-1}}$, $D^{\mathrm{p}}_{\mathrm{Ab}} = D_{\mathrm{Ab}}/5$, see also Table 1.

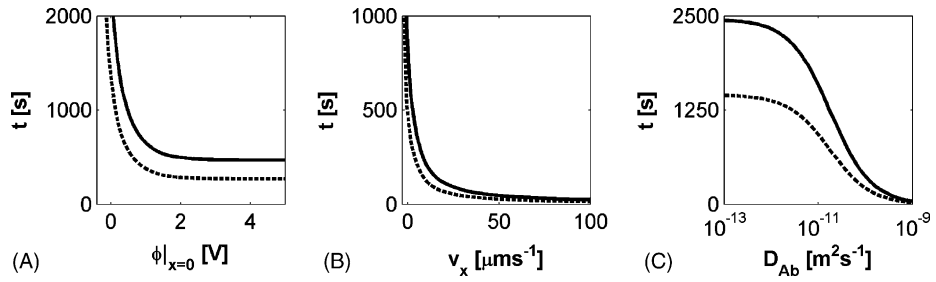

Fig. 4. Dynamical analysis of effects of model parameters on the antigen–antibody complex interactions. Time period necessary to achieve 50% saturation (the dashed line) and 90% saturation (the solid line) of the antigen binding sites. (A) dependence on $\Phi|_{x=0}$, (B) dependence on v_x, (C) dependence on D_{Ab}. The parameter values are (A) $v_x = 1\,\mu m\,s^{-1}$, $D_{Ab} = 5\times10^{-11}\,m^2\,s^{-1}$, (B) $\Phi|_{x=0} = 1\,V$, $D_{Ab} = 5\times10^{-11}\,m^2\,s^{-1}$, (C) $v_x = 1\,\mu m\,s^{-1}$, $\Phi|_{x=0} = 1\,V$. The other model parameters are $q_{fix} = -1\times10^6\,C\,m^{-3}$, $z_{Ab} = 1$, $c_{Ab}|_{x=0} = 4\times10^{-6}\,mol\,m^{-3}$, $D^p_{Ab} = D_{Ab}/5$, see also Table 1.

is a small consumption of the protonized form of the buffer in the dissociation reaction). High level of the fixed negative charge is able to deplete almost all positively charged ions from the input solution. The concentration of the protonized form of the buffer drops to zero near the phase interface and, similarly, the concentration of the chloride anion is low as the system cannot deviate much from the electroneutrality. The resulting conductivity near the interface is very low and thus the electric field intensity has to increase strongly in order to keep the constant flux of the key electrolyte components through the system.

The fixed negative charge has also an effect on the minority ions such as antibody molecules. High intensity of the electric field accelerates (if $z_{Ab} > 0$) transport of the antibody from the input compartment to the reaction compartment. In Fig. 3C, we can observe sharp increase of the antibody concentration near the interface input compartment/reaction compartment ($x^* = 20$).

4.2. Dynamical analysis

Results of the steady-state analysis are quite intuitive. In order to evaluate real capabilities of the proposed ELISA microdevice, we have to study this system from a dynamical point of view. Fast accumulation of the antibody in the reaction environment is the most important property of the system. We define two auxiliary time variables to quantify the dynamical properties of the microdevice: t^{50} and t^{90}. These saturation times correspond to 50 and 90% saturation of the antigen by the antibody molecules in the reaction environment according to

$$\int_0^1 c_c^*(x^*, t^{*50})\,dx^* = 0.5, \quad \text{and}$$
$$\int_0^1 c_c^*(x^*; t^{*90})\,dx^* = 0.9. \tag{11}$$

Let us note that the total concentration of the antigen is 250 times higher than the concentration of the antibody in the inlet electrolyte and the relationship between the dimensional and the dimensionless saturation times is given by a time scaling factor t_0 (see Table 2), e.g., $t^{50} = t_0 t^{*50}$.

The Fig. 4A shows the dependence of saturation times on the voltage applied on the boundary $x^* = 0$. When no potential is applied, the antibody is transported only by diffusion and weak convection ($v_x = 1\,\mu m\,s^{-1}$). Saturation takes more than half an hour. Saturation times sharply increase up to infinity as the value of potential decreases below zero. The required 50 or 90% saturation of antigen is not achieved if a negative potential less than several tenths of volt is imposed. Conversely, a positive potential imposed on the input boundary accelerates the antigen saturation in the reaction compartment due to electrophoretic migration of the antibody with a positive electrostatic charge. Saturation time decreases with the growing potential up to an asymptote given by the limiting current. In the proposed system with negative charge fixed in the porous compartments and positive electrostatic potential on the input boundary, concentrations of all ions near the interface between the input and reaction compartments drop to zero (as explained in the steady-state section). Although the potential on the input boundary increases, the electromigration term of ions near the interface cannot grow due to almost zero ion concentrations. On the other hand, for example, the flow of chloride ions must be kept constant through the entire system. Hence the low ion concentration at the phase interface must be locally compensated by a large electric filed intensity in order to keep the electromigration term on the same level as in the non-interface regions. It means that a higher voltage only increases the potential gradient on the interface with a low electrical conductivity. Existence of the phenomena described above limits a minimal time of the incubation phase to $t^{90} \approx 500\,s$.

The dependence of saturation times on the value of convective velocity is plotted in Fig. 4B. The choice of parameters results in electroosmotic flux of the electrolyte in the positive direction. We can follow a rapid decrease of the saturation times with the increasing velocity. When the intensity of the convective transport dominates, there is no limitation by the limiting current. Hence, the saturation time can steadily decrease to the value of convective velocity where the rate of the antigen–antibody binding reaction becomes limiting. Let us make a rough estimate of this value. Let only the free form of antigen be present in the reaction

compartment; the concentration of the antibody is at the same level as at the input boundary, and the diffusion and electromigration fluxes of the antibody are negligible. Hence the rate of the antigen consumption in the reaction compartment has to be equal to the rate of the antibody supply by convective flux

$$J^{C}_{Ab}|_{x=0} A = -r_c A l_2 \Rightarrow v_x = k_c c_{Ag,tot} l_2. \quad (12)$$

In this case, the limitation of the ELISA process occurs at $v_x \approx 1\,\mathrm{mm\,s^{-1}}$. Velocity of the electroosmotic convection is usually in tens of micrometers per second. Hence the system operates in the regime limited only by the rate of transport.

We can also estimate the saturation time necessary for the incubation period in the regime with dominating convection transport. There are two contributions to the final value of time of incubation: transport through the input compartment (t_{inp}) and the accumulation of the antibody molecules in the reaction compartment (t_{ac})

$$t = t_{inp} + t_{ac} = \frac{l_1}{v_x} + \frac{n_{Ag}}{J^{C}_{Ab}|_{x=0} A} = \frac{(l_1 + l_2 c_{Ag,tot})/c_{Ab}|_{x=0}}{v_x}, \quad (13)$$

here n_{Ag} is the total molar amount of the antigen in the reaction compartment and A the surface area of the probe cross-section. For example, when $v_x = 50\,\mu\mathrm{m\,s^{-1}}$, time of the incubation is approximately 54 s, which agrees with the results of the simulations. Eq. (13) is not valid for low values of convective velocity because of the presence of both the electrophoretic and the diffusion transport. Let us note that time t in Eq. (13) is only a guess of duration of saturation received from analysis of the transport parameters of the system. In a limit case of infinitely fast complex formation, the transport time t of incubation period corresponds to the time of 100% saturation of the antigen binding sites.

The saturation time can be also affected by the diffusion coefficient of the antibody. Both the diffusion and the electromigration fluxes depend on the value of diffusion coefficient. Dependence of the saturation times on values of the diffusion coefficient of the antibody are plotted in Fig. 4C. The dependence has a sigmoidal shape. There is also an asymptote for the saturation time. When the diffusion coefficient of the antibody is very low, the convection transport becomes dominant and Eq. (13), which does not depend on the value of diffusivity, can be applied. On the other hand, if the effective diffusion coefficient of the antibody is high ($D_{Ab} \geq 1 \times 10^{-10}\,\mathrm{m^2\,s^{-1}}$), the antibody molecules are mostly transported by electromigration. The electromigration velocity can be computed from Eq. (4) where the intensity of the imposed electric field at the input boundary is used (as the first approximation, we can assume linear profile of potential through the system). The antibody concentration in the system is much lower than the concentration of the buffer. Thus we can assume that the distribution of the electric field intensity almost does not depend on the accumulation of the antibody in the input and the reaction compartments. If we substitute v_x in Eq. (13) by the expression for the electromigration velocity (Eq. (4)), we receive a formula for evaluation of the saturation times in this limiting case. Let us note that interval of physically relevant values of effective diffusivity of antibody is narrower than in Fig. 4C.

Finally, we have analyzed an entire working cycle of the ELISA probe. The model parameters (see Fig. 5) of this simulation were chosen on the basis of the previous steady-state and dynamical analysis. The working cycle was divided into two parts: the incubation period $t \in (0, 300)$ s and the elution/detection period $t \in (300, 600)$ s. For the incubation period, the distributions of both the antibody concentration on interval $x^* \in \langle 19; 21 \rangle$ (i.e. in the vicinity of the phase interface between the input and reaction compartments) and the antigen–antibody complex in the reaction compartment are plotted in Fig. 5A and D, respectively. The profiles of the antigen concentration show sharp increase close to the phase interface ($x^* = 20$) following from a step change of volume density of the fixed negative charge at the phase interface. The antibody molecules pass the reaction compartment and form the antigen–antibody complex. The level of saturation of the antigen binding sites is plotted in Fig. 5D for the chosen times of the incubation. As we can see, the reaction environment is almost fully saturated by the antibody at $t = 300$ s. Free antibody molecules start to accumulate near the interface of the reaction compartment and the semipermeable membrane. It substantially increases the concentration of the free antibody in the reaction compartment. On the other hand, the antibody concentration near the phase interface remains low due to the depletion of positively charged ions by the negative fixed charge in the reaction compartment.

The polarity of the external electric field (and thus the orientation of the electroosmotic flow) is switched after the saturation of the antigen binding sites ($t = 300$ s). It is evident that the concentration of the antibody molecules quickly approaches zero (see Fig. 5B, $t = 340$ s). This effect is very important for the detection phase. An excess of the free antibody, e.g. tagged by a fluorescence group, is able to disturb the detection of the antigen–antibody complex. The residual low concentration of the antibody at $t = 600$ s is given by the dissociation reaction of the antigen–antibody complex in the reaction compartment. The complex concentration remains high enough during the first 300 s of the elution period (Fig. 5E). The entire elution period is much longer than shown in Fig. 5F because rate of the complex dissociation is low. This effect increases time of prospective regeneration of probe. On the other hand, high complex concentration is necessary for successful detection of the antibody in the sample. Note that the ratio of the scaling factors of the antibody concentration and of the complex concentration is $c_{Ab}|_{x=0}/c_{Ag,tot}$.

For clarity, the time courses of the spatially averaged concentrations of both the antibody and the complex are plotted in Fig. 5C and F. The concentration of the antigen–antibody

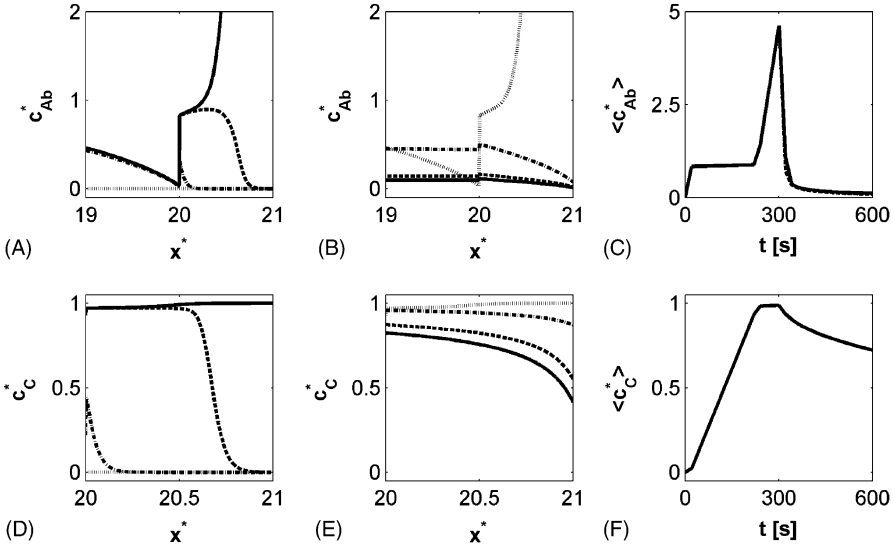

Fig. 5. Analysis of the working cycle of ELISA probe. The plots (A) and (D) show distributions of both the antibody concentration near the interface of the input and the reaction compartments and the complex concentration in the reaction compartment, respectively, in the incubation phase ($t = 0$ s (dotted line), $t = 20$ s (dash-dotted line), $t = 160$ s (dashed line), $t = 300$ s (solid line)). The plots (B) and (E) show the same distributions as the plots (A) and (D) in the elution/detection phase ($t = 300$ s (dotted line), $t = 320$ s (dash-dotted line), $t = 340$ s (dashed line), $t = 600$ s (solid line)). Incubation phase: $\Phi|_{x=0} = 1$ V, $v_x = 10\,\mu\text{m s}^{-1}$; elution phase: $\Phi|_{x=0} = -1$ V, $v_x = -10\,\mu\text{m s}^{-1}$. Time courses (during the complete working cycle) of both the mean antibody concentration in the input and the reaction compartments and the mean complex concentration in the reaction compartment are plotted in (C) and (F), respectively. The boundary concentration of the antibody is $c_{\text{Ab}}|_{x=0} = 4 \times 10^{-6}\,\text{mol m}^{-3}$ during the incubation period. Either $c_{\text{Ab}}|_{x=0} = 4 \times 10^{-6}\,\text{mol m}^{-3}$ (solid line in (C)) or $c_{\text{Ab}}|_{x=0} \to 0\,\text{mol m}^{-3}$ (the dashed line in (C)) is chosen as the antibody boundary condition during the elution period. The other parameters are $D_{\text{Ab}} = 5 \times 10^{-11}\,\text{m}^2\,\text{s}^{-1}$, $D_{\text{Ab}}^{\text{p}} = D_{\text{Ab}}/5$, $q_{\text{fix}} = -1 \times 10^6\,\text{C m}^{-3}$, $z_{\text{Ab}} = 1$, see also Table 1.

complex is averaged over the reaction compartment (interval $x^* \in \langle 20; 21\rangle$) and the concentration of antibody molecules is averaged over both the input and reaction compartments (interval $x^* \in \langle 0; 21\rangle$). The working cycle can be divided into five different periods:

(1) initial period—the antibody molecules are transported from the input boundary to the reaction compartment, $t \in (0, 20)$ s.
(2) saturation period—the antibody molecules bind to the immobilized antigen, $t \in (20, 220)$ s,
(3) accumulation period—an excess of the antibody molecules accumulates in the reaction environment, $t \in (220, 300)$ s,
(4) elution period—the excess of the antibody molecules is transported out of the system, $t \in (300, 340)$ s,
(5) dissociation period—the antibody molecules are released from the complex, $t > 340$ s.

Generally, the dissociation period is very long because of high affinity (equilibrium constant $K_{\text{c}} = 1 \times 10^{-7}\,\text{mol m}^{-3}$) between the antigen and the antibody. Proper change of the electrolyte acidity is one way how to accelerate this process. The dissociation period of the elution phase also depends on the selection of the antibody concentration on the input boundary. For illustration, we have computed the time courses for two limiting cases:

(1) $c_{\text{Ab}}|_{x=0}$ in the elution/detection phase is the same as in the incubation phase ($c_{\text{Ab}}|_{x=0} = 4 \times 10^{-6}\,\text{mol m}^{-3}$),
(2) $c_{\text{Ab}}|_{x=0} \to 0\,\text{mol m}^{-3}$ in the elution/detection phase.

The results of dynamical simulations show that the effect of the antibody concentration on the boundary is negligible during the elution/detection phase (see comparison in Fig. 5C). The entire working cycle is lower than 10 min for the given set of parameters.

5. Conclusions

A typical arrangement of a microchip for an immunoassay application utilizing electric field has been described. This microdevice consists of a main microchannel for sample introduction and of lateral ELISA probes where detection of antibody molecules occurs. Each ELISA probe is composed of input, reaction, semipermeable and output compartments. For this immunoassay chip, we have illustrated possibilities of modeling that uses a simplified description of spatial profiles and transport of biomacromolecules. A formulated mathematical model of the ELISA probe was numerically studied in detail.

First, we have focused on a detailed analysis of steady states in one ELISA probe. Effects of parameters such as antibody diffusivity, antibody charge number, polarity and intensity of an external electric field, convective velocity, and amount of fixed charge in porous compartments on the behavior of the probe were studied. Values of the model parameters giving a large increase of the antibody concentration in the reaction compartment were determined. The steady-state analysis clarified phenomena near phase interfaces such as

formation of an electrical double layer and existence of a limiting current in the system.

Simulations of dynamic behavior of the probe were aimed at finding regions of parameters for short incubation period. The time required for the saturation of the antigen binding sites by the antibody molecules was determined in dependence on three model parameters: the electrostatic potential imposed at the input boundary, the velocity of the electroosmotic flux, and the diffusion coefficient of the antibody. Shapes and asymptotes of these dependences were described by means of simple relationships.

Finally, we have analyzed a complete ELISA cycle (i.e. the incubation and the elution/detection periods) in detail. For modeled conditions, the complete cycle can be realized in less than 10 min.

Acknowledgements

Financial support of this project by the Grant Agency of the Czech Republic (partly grants no. 104/03/D006, 104/01/1319, 104/02/0339) is gratefully acknowledged.

Appendix A. Dimensionless model

Before the implementation of the model into the FEMLAB package, the model Eqs. (1), (6) and (8) were transformed into dimensionless form. The used scaling factors and dimensionless variables and groups are given in Table 2. The mathematical description of the system varies from a compartment to compartment due to different composition of the electrolyte and of the fixed charge in porous media. Eqs. (A.1)–(A.8) can serve as an example of the description of complex reaction-transport problem inside the reaction compartment:

$$\frac{\partial c_{\mathrm{H}}^*}{\partial t^*} = -v^* \frac{\partial c_{\mathrm{H}}^*}{\partial x^*} + D_{\mathrm{H}}^{\mathrm{p}} \frac{\partial^2 c_{\mathrm{H}}^*}{\partial x^{*2}} + D_{\mathrm{H}}^{\mathrm{p}} \frac{\partial}{\partial x^*}\left(c_{\mathrm{H}}^* \frac{\partial \Phi^*}{\partial x^*}\right) + Da_{\mathrm{B}}\left[\frac{K_{\mathrm{b}}}{\sqrt{K_{\mathrm{w}}}} c_{\mathrm{Bp}}^* - c_{\mathrm{H}}^* c_{\mathrm{B}}^*\right] + Da_{\mathrm{H}}(1 - c_{\mathrm{H}}^* c_{\mathrm{OH}}^*), \tag{A.1}$$

$$\frac{\partial c_{\mathrm{OH}}^*}{\partial t^*} = -v^* \frac{\partial c_{\mathrm{OH}}^*}{\partial x^*} + D_{\mathrm{OH}}^{\mathrm{p}} \frac{\partial^2 c_{\mathrm{OH}}^*}{\partial x^{*2}} - D_{\mathrm{OH}}^{\mathrm{p}} \frac{\partial}{\partial x^*}\left(c_{\mathrm{OH}}^* \frac{\partial \Phi^*}{\partial x^*}\right) + Da_{\mathrm{H}}(1 - c_{\mathrm{H}}^* c_{\mathrm{OH}}^*), \tag{A.2}$$

$$\frac{\partial c_{\mathrm{Cl}}^*}{\partial t^*} = -v^* \frac{\partial c_{\mathrm{Cl}}^*}{\partial x^*} + D_{\mathrm{Cl}}^{\mathrm{p}} \frac{\partial^2 c_{\mathrm{Cl}}^*}{\partial x^{*2}} - D_{\mathrm{Cl}}^{\mathrm{p}} \frac{\partial}{\partial x^*}\left(c_{\mathrm{Cl}}^* \frac{\partial \Phi^*}{\partial x^*}\right), \tag{A.3}$$

$$\frac{\partial c_{\mathrm{B}}^*}{\partial t^*} = -v^* \frac{\partial c_{\mathrm{B}}^*}{\partial x^*} + D_{\mathrm{B}}^{\mathrm{p}} \frac{\partial^2 c_{\mathrm{B}}^*}{\partial x^{*2}} + Da_{\mathrm{B}} \frac{\sqrt{K_{\mathrm{w}}}}{c_{\mathrm{B}}|_{x=0}}\left(\frac{K_{\mathrm{b}}}{\sqrt{K_{\mathrm{w}}}} c_{\mathrm{Bp}}^* - c_{\mathrm{H}}^* c_{\mathrm{B}}^*\right), \tag{A.4}$$

$$\frac{\partial c_{\mathrm{Bp}}^*}{\partial t^*} = -v^* \frac{\partial c_{\mathrm{Bp}}^*}{\partial x^*} + D_{\mathrm{Bp}}^{\mathrm{p}} \frac{\partial^2 c_{\mathrm{Bp}}^*}{\partial x^{*2}} + D_{\mathrm{Bp}}^{\mathrm{p}} \frac{\partial}{\partial x^*}\left(c_{\mathrm{Bp}}^* \frac{\partial \Phi^*}{\partial x^*}\right) - Da_{\mathrm{B}} \frac{\sqrt{K_{\mathrm{w}}}}{c_{\mathrm{B}}|_{x=0}}\left(\frac{K_{\mathrm{b}}}{\sqrt{K_{\mathrm{w}}}} c_{\mathrm{Bp}}^* - c_{\mathrm{H}}^* c_{\mathrm{B}}^*\right), \tag{A.5}$$

$$\frac{\partial c_{\mathrm{Ab}}^*}{\partial t^*} = -v^* \frac{\partial c_{\mathrm{Ab}}^*}{\partial x^*} + D_{\mathrm{Ab}}^{\mathrm{p}} \frac{\partial^2 c_{\mathrm{Ab}}^*}{\partial x^{*2}} + D_{\mathrm{Ab}}^{\mathrm{p}} z_{\mathrm{Ab}} \frac{\partial}{\partial x^*}\left(c_{\mathrm{Ab}}^* \frac{\partial \Phi^*}{\partial x^*}\right) + Da_{\mathrm{C}}\left(\frac{K_{\mathrm{c}}}{c_{\mathrm{Ab}}|_{x=0}} c_{\mathrm{C}}^* - c_{\mathrm{Ab}}^*(1 - c_{\mathrm{C}}^*)\right), \tag{A.6}$$

$$\frac{\partial c_{\mathrm{C}}^*}{\partial t^*} = -Da_{\mathrm{C}} \frac{c_{\mathrm{Ab}}|_{x=0}}{c_{\mathrm{Ag,tot}}}\left(\frac{K_{\mathrm{c}}}{c_{\mathrm{Ab}}|_{x=0}} c_{\mathrm{C}}^* - c_{\mathrm{Ab}}^*(1 - c_{\mathrm{C}}^*)\right), \tag{A.7}$$

$$\frac{\partial^2 \Phi^*}{\partial x^{*2}} = -G\left[\frac{\sqrt{K_{\mathrm{w}}}}{c_{\mathrm{B}}|_{x=0}}(c_{\mathrm{H}}^* - c_{\mathrm{OH}}^*) - c_{\mathrm{Cl}}^* + c_{\mathrm{Bp}}^* + \frac{c_{\mathrm{Ab}}|_{x=0}}{c_{\mathrm{B}}|_{x=0}} z_{\mathrm{Ab}} c_{\mathrm{Ab}}^* + \frac{c_{\mathrm{Ag,tot}}}{c_{\mathrm{B}}|_{x=0}} z_{\mathrm{Ab}} c_{\mathrm{C}}^* + Q\right]. \tag{A.8}$$

References

[1] E.P. Diamandis, T.K. Christopoulus, Immunoassay, Academic Press, New York, 1997.
[2] M.J. Heller, A. Guttman, Integrated Microfabricated Biodevices, Marcel Dekker, New York, 2002.
[3] P.G. Righetti, C. Gelfi, M.R. D'Acunto, Electrophoresis 23 (2002) 1361–1374.
[4] N.A. Guzman, S.S. Park, D. Schaufelberger, L. Hernandez, X. Paez, P. Rada, A.J. Tomlinson, S. Naylor, J. Chromatogr. B 697 (1997) 37–66.
[5] A. Dodge, K. Fluri, E. Verpoorte, N.F. de Rooij, Anal. Chem. 73 (2001) 3400–3409.
[6] K. Dill, D.D. Montgomery, W. Wang, J.C. Tsai, Anal. Chim. Acta 444 (2001) 69–78.
[7] K.L. Ewalt, R.W. Haigis, R. Rooney, D. Ackley, M. Krihak, Anal. Biochem. 289 (2001) 162–172.
[8] J.S. Rossier, H.H. Girault, Lab. Chip 1 (2001) 153–157.
[9] J. Rossier, F. Reymond, P.E. Michel, Electrophoresis 23 (2002) 858–867.
[10] S.B. Cheng, C.D. Skinner, J. Taylor, J. Attiya, W.E. Lee, G. Picelli, D.J. Harrison, Anal. Chem. 73 (2001) 1472–1479.
[11] A.E. Herr, J.I. Molho, K.A. Drouvalakis, J.C. Mikkelsen, P.J. Utz, J.G. Santiago, T.W. Kenny, Anal. Chem. 75 (2003) 1180–1187.
[12] R.M. Guijt, E. Baltussen, G.W.K. van Dedem, Electrophoresis 23 (2002) 823–835.
[13] K. Sato, A. Hibara, M. Tokeshi, H. Hisamoto, T. Kitamori, Anal. Sci. 19 (2003) 15–22.

[14] K. Sato, A. Hibara, M. Tokeshi, H. Hisamoto, T. Kitamori, Adv. Drug Delivery Rev. 55 (2003) 379–391.
[15] S.V. Ermakov, S.C. Jacobson, J.M. Ramsey, Anal. Chem. 70 (1998) 4494–4504.
[16] S.V. Ermakov, S.C. Jacobson, J.M. Ramsey, Anal. Chem. 72 (2000) 3512–3517.
[17] D. Li, Colloids Surf. A 195 (2001) 35–57.
[18] J. Lindner, D. Šnita, M. Marek, Phys. Chem. Chem. Phys. 4 (2002) 1348–1354.
[19] J. Khandurina, S.C. Jacobson, L.C. Waters, R.S. Foote, J.M. Ramsey, Anal. Chem. 71 (1999) 1815–1819.
[20] R.F. Probstein, Physicochemical Hydrodynamics: An Introduction, 2nd ed., Wiley, New York, 1994.